Short Article

Cell Stem Cell

Quantitative Clonal Analysis and Single-Cell Transcriptomics Reveal Division Kinetics, Hierarchy, and Fate of Oral Epithelial Progenitor Cells

Graphical Abstract

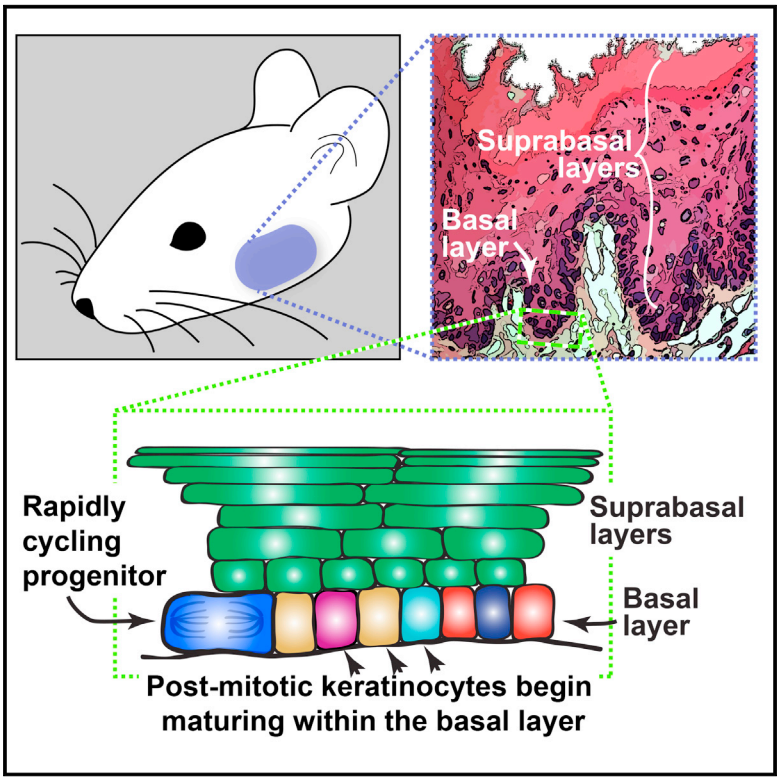

Highlights

- Oral mucosal progenitor cells are located in the basal layer and proliferate rapidly
- *Bmi1* is expressed by nearly all basal layer cells, including oral mucosal progenitors
- Progenitors undergo population-asymmetric self-renewal with neutral drift dynamics
- Single-cell RNA-seq reveals a continuum of cell maturation states in the basal layer

Authors

Kyle B. Jones, Sachiko Furukawa, Pauline Marangoni, ..., Rapolas Zilionis, Allon M. Klein, Ophir D. Klein

Correspondence

ophir.klein@ucsf.edu

In Brief

Jones et al. define the organization, cycling kinetics, and clonal dynamics of oral mucosal progenitor cells. They also show, via single-cell RNA sequencing, that the basal layer contains progenitor and post-mitotic cells at various stages of maturation, demonstrating basal layer heterogeneity and providing insights into localization of cell fate decisions.

Jones et al., 2019, Cell Stem Cell *24*, 1–10
January 3, 2019 © 2018 Elsevier Inc.
https://doi.org/10.1016/j.stem.2018.10.015

CellPress

Please cite this article in press as: Jones et al., Quantitative Clonal Analysis and Single-Cell Transcriptomics Reveal Division Kinetics, Hierarchy, and Fate of Oral Epithelial Progenitor Cells, Cell Stem Cell (2018), https://doi.org/10.1016/j.stem.2018.10.015

Cell Stem Cell
Short Article

CellPress

Quantitative Clonal Analysis and Single-Cell Transcriptomics Reveal Division Kinetics, Hierarchy, and Fate of Oral Epithelial Progenitor Cells

Kyle B. Jones,[1] Sachiko Furukawa,[1,2,10] Pauline Marangoni,[1,10] Hongfang Ma,[1,3] Henry Pinkard,[4,5,6] Rebecca D'Urso,[1] Rapolas Zilionis,[7,8] Allon M. Klein,[7] and Ophir D. Klein[1,9,11,*]

[1]Program in Craniofacial Biology and Department of Orofacial Sciences, University of California, San Francisco, San Francisco, CA, USA
[2]Section of Oral and Maxillofacial Oncology, Faculty of Dental Science, Kyushu University, Fukuoka, Japan
[3]Department of Plastic and Reconstructive Surgery, Sir Run Run Shaw Hospital, Zhejiang University School of Medicine, Zhejiang, China
[4]Department of Pathology, University of California, San Francisco, San Francisco, CA, USA
[5]Biological Imaging Development Center, University of California, San Francisco, San Francisco, CA, USA
[6]Computational Biology Graduate Group, University of California, San Francisco, San Francisco, CA, USA
[7]Department of Systems Biology, Harvard Medical School, Boston, MA, USA
[8]Vilnius University Institute of Biotechnology, Vilnius, Lithuania
[9]Department of Pediatrics and Institute for Human Genetics, University of California, San Francisco, San Francisco, CA, USA
[10]These authors contributed equally
[11]Lead Contact
*Correspondence: ophir.klein@ucsf.edu
https://doi.org/10.1016/j.stem.2018.10.015

SUMMARY

The oral mucosa is one of the most rapidly dividing tissues in the body and serves as a barrier to physical and chemical insults from mastication, food, and microorganisms. Breakdown of this barrier can lead to significant morbidity and potentially life-threatening infections for patients. Determining the identity and organization of oral epithelial progenitor cells (OEPCs) is therefore paramount to understanding their roles in homeostasis and disease. Using lineage tracing and label retention experiments, we show that rapidly dividing OEPCs are located broadly within the basal layer of the mucosa throughout the oral cavity. Quantitative clonal analysis demonstrated that OEPCs undergo population-asymmetrical divisions following neutral drift dynamics and that they respond to chemotherapy-induced damage by altering daughter cell fates. Finally, using single-cell RNA-seq, we establish the basal layer population structure and propose a model that defines the organization of cells within the basal layer.

INTRODUCTION

For several decades, the epidermal proliferative unit (EPU) hypothesis, also known as the invariant asymmetry model, was used to describe the organization of stem cells within the epidermis and oral mucosa. In this model, single stem cells within the basal layer divide slowly and asymmetrically, always resulting in a stem cell and a daughter transit-amplifying cell, which remain closely associated with one another and are organized in stem cell-transit amplifying cell territories or progenitor units (Mackenzie, 1997; Potten, 1974). More recently, studies in several epithelial tissues, such as the epidermis and esophagus, support the alternative population asymmetry model, in which the basal layer consists of a single pool of progenitor cells along with post-mitotic cells fated for differentiation (Figures S1A and S1B; Clayton et al., 2007; Doupé et al., 2012). Although prior work in the tongue epithelium supported the invariant asymmetry model, based in part on the suggestion that solitary stem cells express high levels of *Bmi1* within the dorsal tongue epithelium (Tanaka et al., 2013), quantitative clonal analysis to confirm this finding has not yet been performed. In this study, we sought to identify and characterize oral epithelial progenitor cells (OEPCs) in all oral mucosal sites, determine how they are organized, study the effects that aging and cytotoxic damage have on their behavior, and resolve which model—invariant asymmetry or population asymmetry—best explains their division kinetics and clonal growth patterns.

RESULTS

Bmi1 Labels Basal Oral Epithelial Cells, Including Oral Epithelial Progenitors

A prior study in keratinocytes within the dorsal tongue epithelium using *in situ* hybridization (ISH) and lineage tracing techniques reported that *Bmi1* is highly expressed by rare, solitary stem cells primarily in the suprabasal layer (Tanaka et al., 2013). Therefore, we initially set out to determine whether *Bmi1* labeled rare OEPCs at other oral mucosal sites by using RNAscope, a sensitive and specific ISH method. Surprisingly, we found that *Bmi1* was expressed at low levels in almost all basal and some suprabasal layer keratinocytes at various oral mucosal sites, including the dorsal tongue (Figures 1A and 1B and S1D–S1I). We next used $Bmi1^{CreER}$;$R26^{tdTomato}$ mice to verify that *Bmi1*-expressing keratinocytes were located primarily within the basal layer and to determine whether *Bmi1* also labeled OEPCs. Following a single

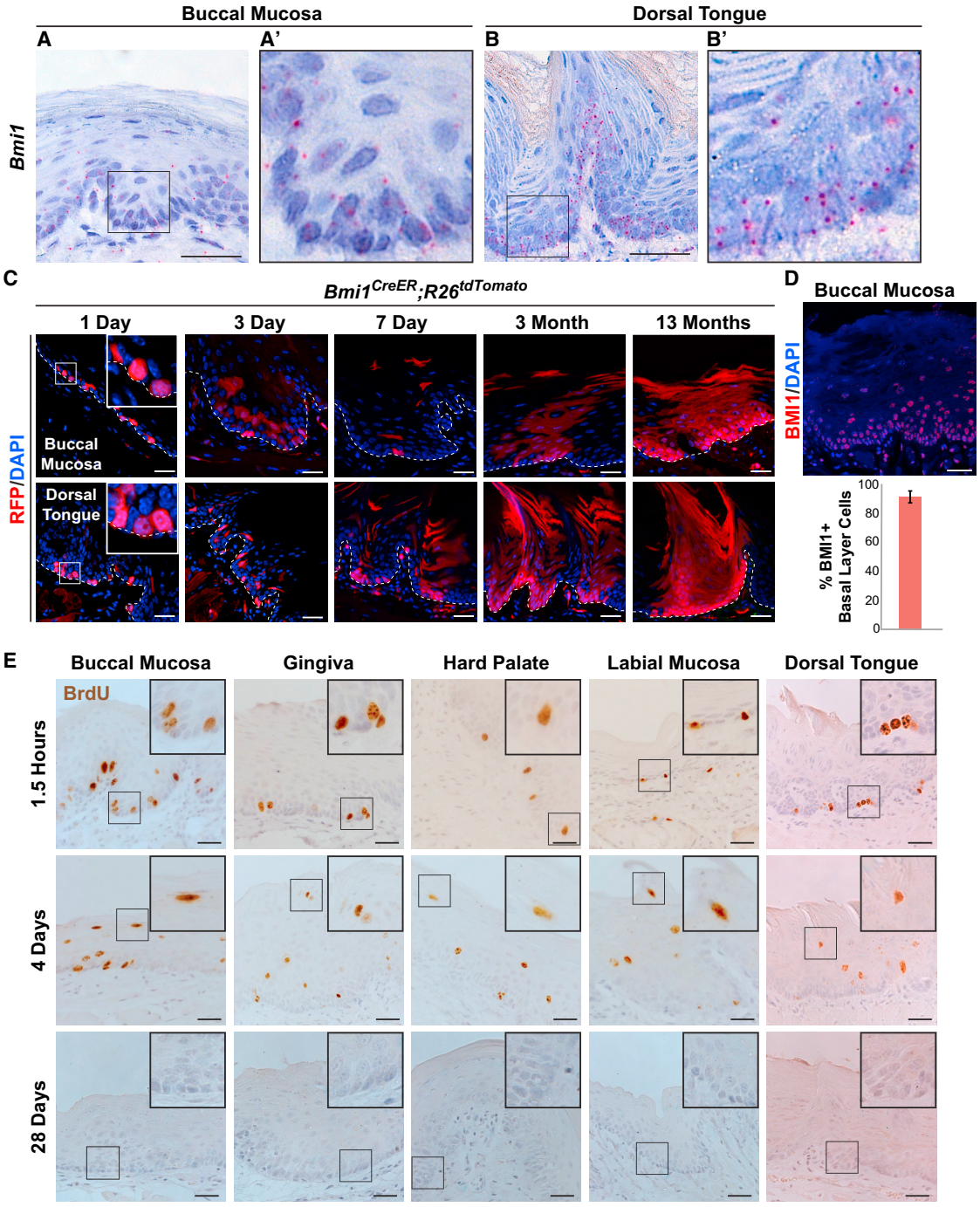

Figure 1. *Bmi1* Labels Progenitor Cells within the Rapidly Dividing Basal Layer of the Oral Mucosa

(A and B) *Bmi1* RNAscope ISH experiments (individual transcripts are represented by red dots) in the buccal mucosa (A) and dorsal tongue (B).

(C) $Bmi1^{CreER};R26^{tdTomato}$ mice following administration of a single low dose of tamoxifen. Dashed white line represents the epithelial/connective tissue interface.

(D) BMI1 protein expression.

(E) Various oral mucosal sites in mice injected with BrdU and euthanized 1.5 hr, 4 days, or 28 days later.

Scale bars, 30 μm.

dose of tamoxifen and 24-hr chase, labeled keratinocytes were found almost exclusively in the basal layer throughout the oral mucosa (Figure 1C), confirming our *Bmi1* ISH assay. Furthermore, in contrast to the previous report of solitary *Bmi1*-expressing keratinocytes within the tongue (Tanaka et al., 2013), multiple *Bmi1*-expressing keratinocytes were identified, often in close proximity to one another (Figure 1C). Labeling throughout the oral mucosa persisted for up to 13 months, confirming that at

least some of the *Bmi1*-expressing cells were long-lived OEPCs. Immunofluorescence showed BMI1 protein expression in most basal cells (90.4% of cells, SD 4.1%) and many suprabasal layer cells (Figure 1D). We also induced other *CreER* mouse lines driven by *Krt14*, *Gli1*, *Sox2*, and *Lrig1* and found that, similar to *Bmi1,* these drivers labeled OEPCs in the basal layer and showed labeling that persisted for at least 3 to 6 months (Figures S3A–S3F). These findings strongly suggest that OEPCs are located within the basal layer of the oral mucosa and not in the suprabasal layer, as proposed previously (Tanaka et al., 2013). Additionally, in contrast to other tissues, *Bmi1* does not appear to be a specific marker of progenitors in the oral mucosa given its broad expression in most basal layer cells.

Oral Mucosal Basal Layer Cells Actively Proliferate, Leading to Rapid Tissue Turnover

We next determined the division kinetics of basal layer keratinocytes by injecting wild-type mice with 5-bromo-2′-deoxyuridine (BrdU) and euthanizing them at various time points (Figure 1E). 1.5 hr post-injection, BrdU-labeled keratinocytes were detected predominantly in the basal layer, confirming this layer as the primary site of cell division within the oral mucosa. By day 4, BrdU-labeled keratinocytes were present in the *stratum corneum*, consistent with rapid turnover of the oral mucosa. By day 28, only a few rare cells with the BrdU label remained in the tissue, indicating that those basal layer keratinocytes that were labeled 1 month prior had divided multiple times and/or left the basal layer (Figure S1C). In light of the similar rates of turnover in the various regions of the oral mucosa (Figure 1E), we focused our analysis on the buccal epithelium, which provides a large expanse of tissue. Consistent with the rapid loss of BrdU, approximately 95% of basal layer keratinocytes in the buccal mucosal epithelium of wild-type mice expressed Ki-67, a marker of proliferating cells that is also retained in newly post-mitotic cells. These data are consistent with the notion that many basal layer cells are proliferating and that post-mitotic cells do not remain in the basal layer for more than a few days after cell cycle exit (Figures 2A and 2B and S1K–S1M; Mendeley Figure S1A and S1B).

Label-Retaining Cells Are Not Present in the Basal Layer of the Oral Mucosa

Classically, label retention was considered a hallmark of adult stem cells, and *Bmi1*-positive keratinocytes in the dorsal tongue epithelium have been reported to be slow-cycling (Tanaka et al., 2013). However, it is now clear that many adult stem cell populations are proliferative as opposed to quiescent (Doupé et al., 2012; Li and Clevers, 2010). We therefore assessed whether label-retaining cells (LRCs) reside in the buccal mucosal epithelium using the $K5^{tTa}$;*tetO-H2B*^{GFP} system (Tumbar et al., 2004). Mice were euthanized at various time points following doxycycline treatment, and, using the same imaging parameters for each sample, we found a nearly complete loss of EGFP signal by day 21 in the buccal mucosa (Figure 2C). When imaging parameters were optimized to detect EGFP, extremely rare EGFP-positive keratinocytes were present at the 6-week and 3-month chases (Figure 2D). These cells were not arranged in any regular pattern, in contrast to what would be expected with the EPU hypothesis (Figure S1A). Furthermore, the fluorescence intensity of these cells fell below the first percentile values measured in baseline keratinocytes (i.e., no doxycycline treatment), indicating that they had divided multiple times and were not true LRCs (Table S1). Consistent with the BrdU and Ki-67 data, these results indicate that OEPCs rapidly proliferate and that post-mitotic cells within the basal layer remain there for only a brief period.

Division Kinetics of Oral Mucosal Basal Layer Cells

To analyze the division kinetics further, we used dual BrdU/5-ethynyl-2′-deoxyuridine (EdU) labeling (Martynoga et al., 2005) to calculate the average lengths of the S phase and cell cycle in basal layer keratinocytes, which were 2.5 and 49 hr, respectively (Figures 2E, 2F, and S2A–S2C); S phase lengths as brief as 1.8 hr have been reported in mammalian cells (Arai et al., 2011). To measure the average doubling time of OEPCs within the basal layer, we calculated fluorescence decay rates in baseline, 3-day, and 7-day $K5^{tTa}$;*tetO-H2B*^{GFP} samples (Figures 2G, 2H, and S2D). The average decay rate correlated with a doubling time of approximately 45 hr, similar to the cell cycle length of 49 hr. To confirm this, wild-type mice were injected with BrdU at baseline and with EdU at 48 hr and then euthanized 3 hr later (Figure 2I). Approximately 20% of cells (SD 2.5%, n = 447 cells) in the buccal mucosal epithelium showed dual staining for both BrdU and EdU, confirming their reentry into the cell cycle within 48 hr. These findings indicate that proliferating basal layer keratinocytes continually and rapidly enter the cell cycle, on average about once every 2 days. This rapid turnover results in a lack of LRCs, arguing against the invariant asymmetry model.

OEPCs Undergo Population-Asymmetric Self-Renewal with Neutral Drift Dynamics

We next used quantitative clonal analysis to determine whether OEPCs divided via invariant or population asymmetry. 3-month-old *Bmi1*^{CreER};*R26*^{tdTomato} mice were injected with low-dose tamoxifen to induce sparse single-cell labeling, and clones were analyzed at various time points via whole-mount imaging (Figures 3A–3H and S3G; Mendeley Figure S1C). The number of labeled clones as well as the total number of labeled basal layer keratinocytes within each clone were quantified. We found that the overall number of clones in both the buccal and dorsal tongue epithelia decreased over time, whereas the number of labeled basal layer keratinocytes within surviving clones increased linearly with time, consistent with the population asymmetry model (Figure S1B). Further, a quantitative fit to a model of neutral drift used previously to model epidermal keratinocytes (Clayton et al., 2007; Klein et al., 2007) predicted that half of the cells in the basal layer were dividing and that the other half were post-mitotic, with a short residence time comparable in duration with the cell cycle of OEPCs (STAR Methods).

Aged OEPCs Show Decreased Proliferative Capacity

Damaged oral mucosa regenerates more rapidly in younger versus older individuals (Engeland et al., 2006). To understand what role OEPCs might have in this process, we performed quantitative clonal analysis in the buccal mucosa of 15- to 19-month-old *Bmi1*^{CreER};*R26*^{tdTomato} mice (Figures S3H–S3J). Interestingly, although we found clonal labeling patterns similar to those in younger mice, the older mice showed an approximately 50% reduction in the average number of labeled basal

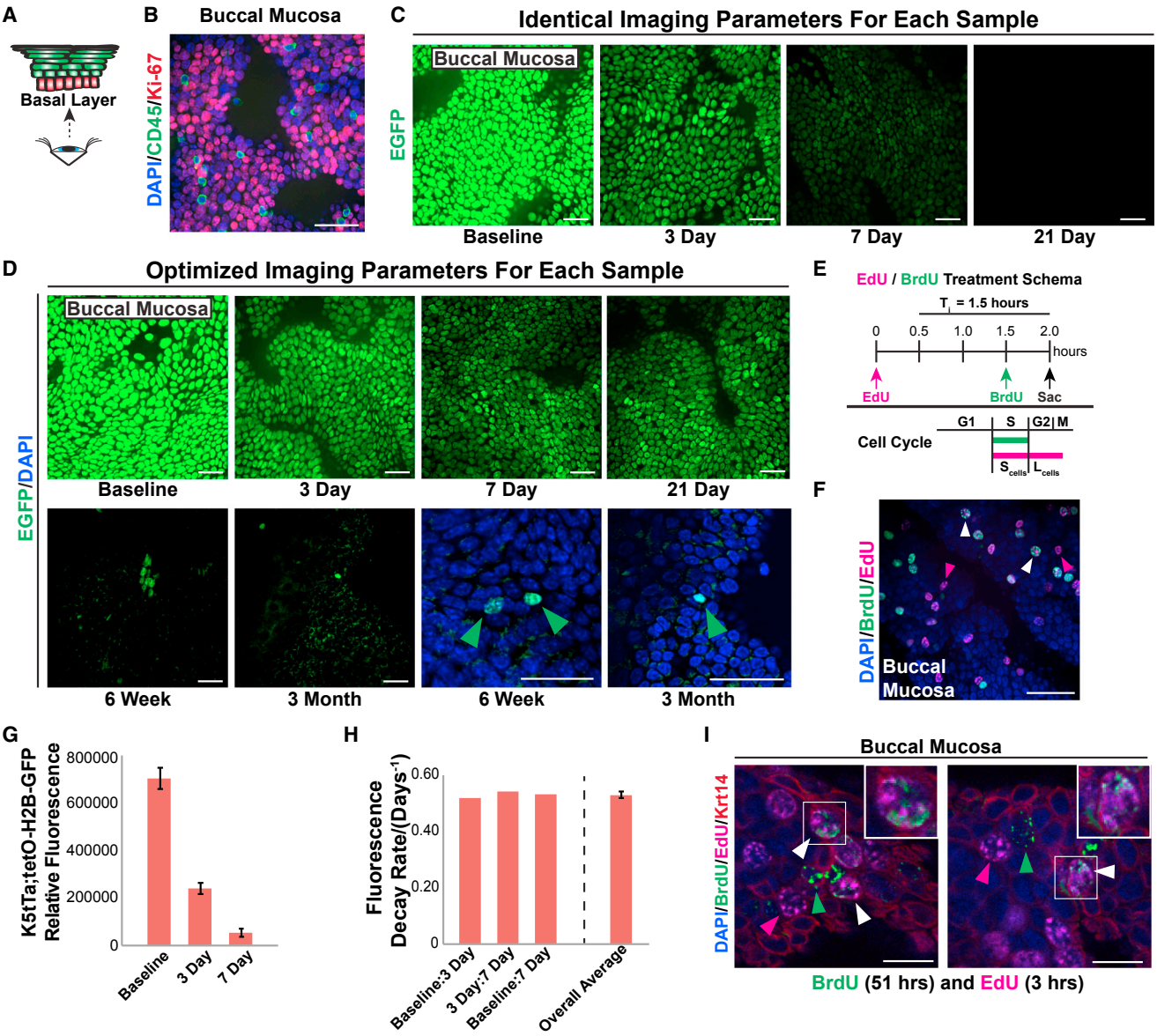

Figure 2. The Buccal Mucosa Does Not Contain Label-Retaining Cells and Exhibits Rapid Cell Division Rates

(A) Schematic view of sample orientation.

(B) Ki-67 protein expression using whole-mount imaging in 10-week-old C57BL/6J mice. CD45+ immune cells were excluded from the analysis. Scale bars, 30 μm.

(C) Whole-mount imaging of buccal epithelium from *K5^{tTa}; tetO-H2B^{GFP}* mice following administration of doxycycline to shut off H2B-EGFP expression using the same imaging parameters for each sample.

(D) Optimized imaging parameters to maximize the detectable EGFP signal in the same samples from (C). Scale bars, 30 μm.

(E and F) Temporally spaced pulses of EdU and BrdU (E) used to calculate the average S phase and total cell cycle times. Keratinocytes that exit S phase prior to euthanasia will only be labeled with EdU (pink arrowheads, F), whereas keratinocytes still within S phase will be labeled with both EdU and BrdU (white arrowheads, F); see STAR Methods for further details. Scale bar, 30 μm.

(G and H) The total relative fluorescence of individual keratinocytes from the samples imaged in (C) were measured, and the fluorescence decay rates were calculated. Bar graphs represent average cell fluorescence values ± SD at each chase time point (G) and the overall average decay rate ± SD (H).

(I) Whole-mount imaging of buccal epithelium after a 48-hr pulse with BrdU followed by a 3-hr pulse with EdU showing BrdU/EdU dual-labeled keratinocytes (white arrowheads) along with keratinocytes that are labeled with only BrdU (green arrowheads) or EdU (red arrowheads).

Scale bars, 10 μm.

layer keratinocytes per clone (although this was not statistically significant; $p = 0.24$; Figure 3I). Further, in the buccal epithelium of 18- to 19-month-old mice, only 63% of basal layer keratinocytes expressed Ki-67, compared with 95% in younger mice ($p < 0.00001$; Figures 3J, 3K, and S3K). These results indicate that, as mice age, the fraction of OEPCs within the basal layer and/or their proliferative capacity decreases, which could explain why oral mucosal damage in older human patients takes

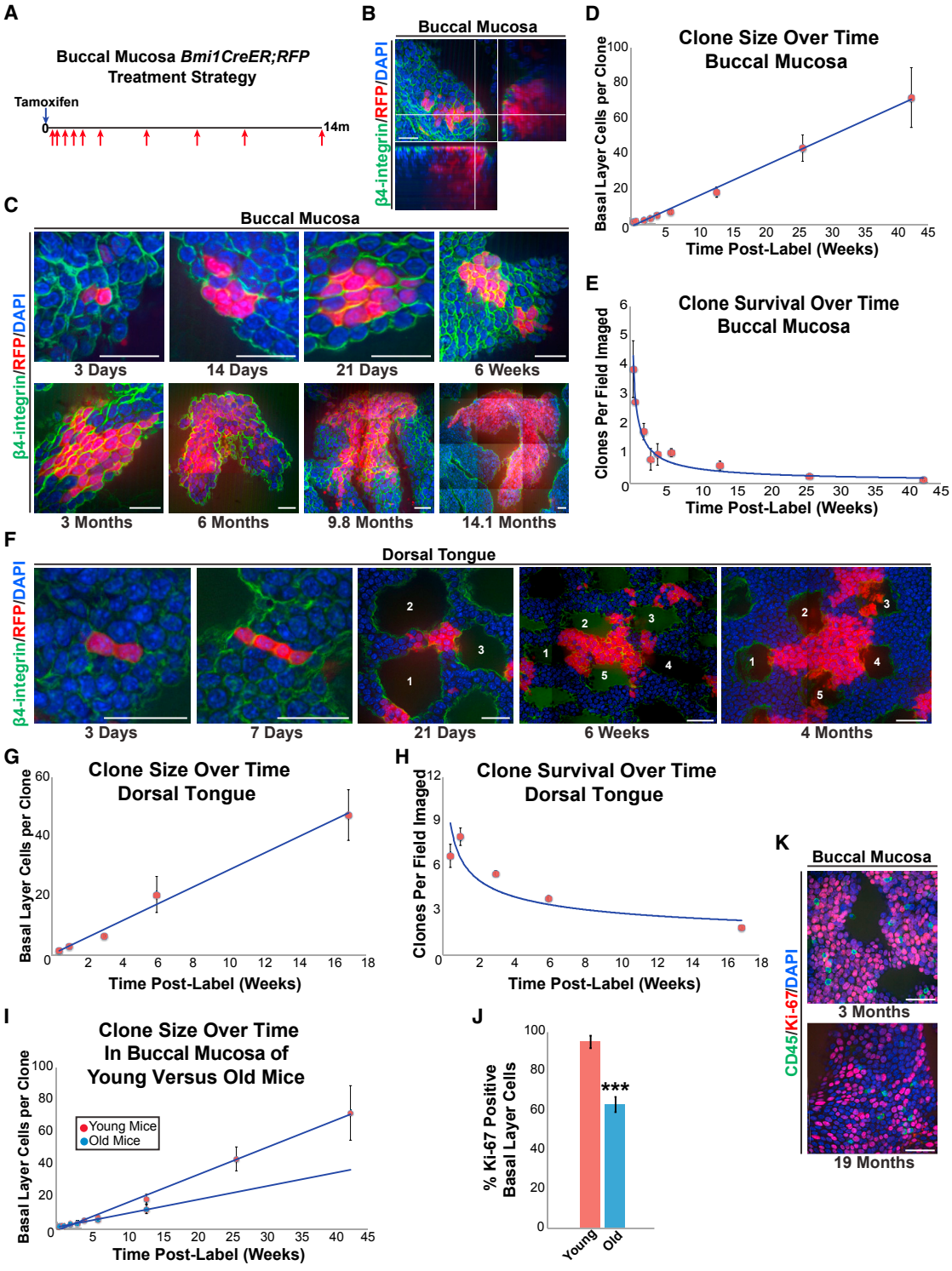

Figure 3. *Bmi1*-Labeled OEPCs in the Buccal Mucosa and Dorsal Tongue Divide via Population Asymmetry with Neutral Drift Dynamics

(A) 2- to 3-month-old *Bmi1*^{CreER};*R26*^{tdTomato} mice were given a single dose of tamoxifen and chased up to 14 months.

(B and C) Whole-mount imaging of labeled clones in buccal mucosal epithelial sheets (B) at multiple time points (C); the number of clones containing at least one labeled basal layer keratinocyte was quantified, along with the number of labeled basal layer keratinocytes present within each clone. Scale bars, 20 μm.

(D and E) As predicted by the population asymmetry model with neutral drift dynamics, the number of labeled basal layer keratinocytes per clone increased over time (D, 1.7 cells/week ± 0.08 SE), whereas the overall number of clones decreased (E, 0.22 clones/tile/week ± 0.03 SE). Data points represent mean values ± SD. Solid curves show neutral drift predictions of linear growth of the average (D) and inverse linear decay of the labeling density (E).

(legend continued on next page)

longer to heal, analogous to age-related changes seen in other tissues (Keyes et al., 2013).

5-Fluorouracil-Induced Cytotoxic Damage Causes OEPCs to Alter Their Daughter Cell Fates

With an understanding of how OEPCs behave under normal steady-state conditions, we next addressed their response to cytotoxic damage. We injected mice with 5-fluorouracil (5FU), a pyrimidine analog used to treat cancer that induces oral mucositis in humans and acts primarily by inhibiting thymidylate synthase, leading to cell cycle arrest and/or apoptosis (Baydar et al., 2005). *Bmi1*^{CreER};*R26*^{tdTomato} mice were first injected with tamoxifen to label OEPCs and then treated with either saline or 5FU once daily for 3 consecutive days, and then clones were analyzed at various time points (Figure 4A). Within the buccal mucosa, 1 day post-5FU, we detected a significant decrease in basal layer cell density ($p = 0.0002$) and mitotic activity ($p = 0.03$; Figures 4C and 4D) as well as an increase in p53 protein levels over several days, confirming that 5FU had damaged basal layer cells (Figure S4A). Surprisingly, basal layer keratinocytes never switched to a hyper-proliferative state following 5FU-induced damage but, instead, slowly returned to normal mitotic activity between 14 and 21 days after treatment (Figure 4D). Despite their slow mitotic recovery, by 3 days post-5FU, treated mice showed significantly larger average clone sizes compared with controls, which persisted through day 21 of the experiment ($p < 0.001$; Figures 4E and 4F).

We next addressed the seemingly paradoxical observation that 5FU-treated mice had a decreased mitotic index but still produced clones with increased numbers of labeled basal layer keratinocytes. One potential scenario consistent with this observation would be that 5FU damage caused OEPCs to preferentially self-renew and replace damaged basal layer keratinocytes instead of creating daughter cells fated for differentiation. To test this, we measured the percentage of labeled basal and suprabasal keratinocytes in control and 5FU-treated mice and found that, by 3 days post-5FU, treated mice had significantly fewer labeled suprabasal cells ($p < 0.001$; Figure 4G). 5FU-treated mice also exhibited a small but significant increase in the number of parallel-oriented mitotic figures (i.e., both daughter cells remained in the basal layer; $p = 0.01$; Figures S4B–S4D). These results demonstrate that OEPCs compensate for tissue damage within the basal layer by altering their daughter cell fates.

Single-Cell RNA-Seq Establishes the Population Structure of Oral Epithelial Basal Layer Cells

Finally, we used an unbiased single-cell RNA sequencing (scRNA-seq) approach to determine the overall diversity of cells residing within the oral mucosal basal layer and to infer lineage relationships. We sorted buccal mucosal basal layer keratinocytes (in two technical replicates) and, following data filtering, identified 16,572 cells that formed a continuum of cell states that we partitioned into 8 distinct cell clusters, which were visualized using SPRING (Weinreb et al., 2018). To explore the phenotype of each cluster, we performed a gene enrichment analysis with emphasis on transcription factors (Tables S2 and S3; Figures S4E–S4J). We found that clusters 1 and 2 represented OEPCs (enriched for basal/progenitor markers), cluster 3 represented cells in G1/S or G2/M (enriched for cell cycle genes), and cells from clusters 4–8 were at various stages of differentiation (enriched for keratinocyte differentiation markers; Figure 4H).

Cluster 1 comprised the majority of OEPCs identified from the ~16,500 cells analyzed (4,712 cells, 28%), whereas cluster 2 was much smaller (140 cells, 0.8%). Both clusters showed high expression of basal/progenitor markers (*Krt5*, *Krt14*, and *Krt15*), enrichment of factors required for stem cell maintenance (*Ascl2*, *Tfcp2l1*, *Procr*, and *Patz1*), and enrichment of members of the Wnt and Notch pathways (Tables S2 and S3). Several other Wnt genes were also expressed at high levels (Figures 4I and S4H).

We further evaluated the expression patterns of *Sox2*, *Lrig1*, *Bmi1*, *Krt14*, and *Gli1*, genes that labeled OEPCs, as we had shown previously (Figure S4G). Although only *Krt14* and *Gli1* were enriched within specific clusters, all five genes were expressed broadly among both OEPCs and post-mitotic differentiating cells. Thus, these genes are not unique to OEPCs and are expressed broadly within the basal layer. For practical purposes, because droplet scRNA-seq has an mRNA detection efficiency of under 10% per molecule in several protocols (Klein et al., 2015; Liu and Trapnell, 2016; Macosko et al., 2015), the expression of these genes at the individual cell level may be underestimated in this analysis. This likely explains why *Bmi1* is not identified in all cells, as would be predicted based on the ISH results.

Cluster 3 cycling cells (5,259 cells, 32%) expressed numerous transcription factors associated with G1/S and G2/M phases of the cell cycle. Cells from clusters 5 (3,726 cells, 22%), 4 (2,195 cells, 13%), and 7 (76 cells, 0.4%) showed a stepwise increase in the expression of *Krt4*, *Krt13*, *Lor*, *Krtdap*, and other genes associated with epidermal differentiation as well as a stepwise decrease in OEPC markers such as *Krt14* and *Krt5* (Figure 4I). Interestingly, cluster 6 cells (414 cells, 2.5%) also expressed differentiation markers but had a strong inflammatory gene signature (specifically, interferon-induced genes secondary to viral infection), thus likely representing virally infected oral epithelial cells. Cluster 8 cells (50 cells, 0.3%) expressed keratinocyte differentiation genes as well as high levels of *Krt14*, which is normally only enriched within OEPCs, as well as markers of wound healing,

(F) Similar clonal labeling patterns were observed in the dorsal tongue epithelium of *Bmi1*^{CreER};*R26*^{tdTomato} mice. Many clones at early chase time points were associated with up to three dorsal tongue papillae (numbered 1–3), whereas, at later time points, they were associated with as many as 5 papillae (numbered 1–5). Scale bars, 20 μm.

(G and H) Dorsal tongue clone size (G, increase of 2.8 cells/week ± 0.20 SE) and clone survival patterns over time (H, loss of 0.03 clones/tile/week ± 0.0009 SE) were similar to those found in the buccal mucosa. Data points represent mean values ± SD. Solid curves show neutral drift predictions for growth within clones and clone survival over time.

(I) Clonal analysis of the buccal mucosa from 15-month-old *Bmi1*^{CreER};*R26*^{tdTomato} mice showed similar clonal growth patterns over time as seen in the 2- to 3-month-old mice; however, the OEPC competition rate in the older mice was halved compared with the younger mice (increase of 0.85 cells/week ± 0.06 SE versus 1.7 cells/week ± 0.08 SE). Data points represent mean values ± SD. Solid lines represent the neutral drift predictions for clonal growth.

(J and K) Whole-mount imaging of buccal mucosa revealed that old mice had significantly fewer Ki-67 positive cells (***$p < 0.00001$). Bar graphs represent the average percent of basal layer keratinocytes that were Ki-67 positive ± SD. Scale bars, 30 μm.

Please cite this article in press as: Jones et al., Quantitative Clonal Analysis and Single-Cell Transcriptomics Reveal Division Kinetics, Hierarchy, and Fate of Oral Epithelial Progenitor Cells, Cell Stem Cell (2018), https://doi.org/10.1016/j.stem.2018.10.015

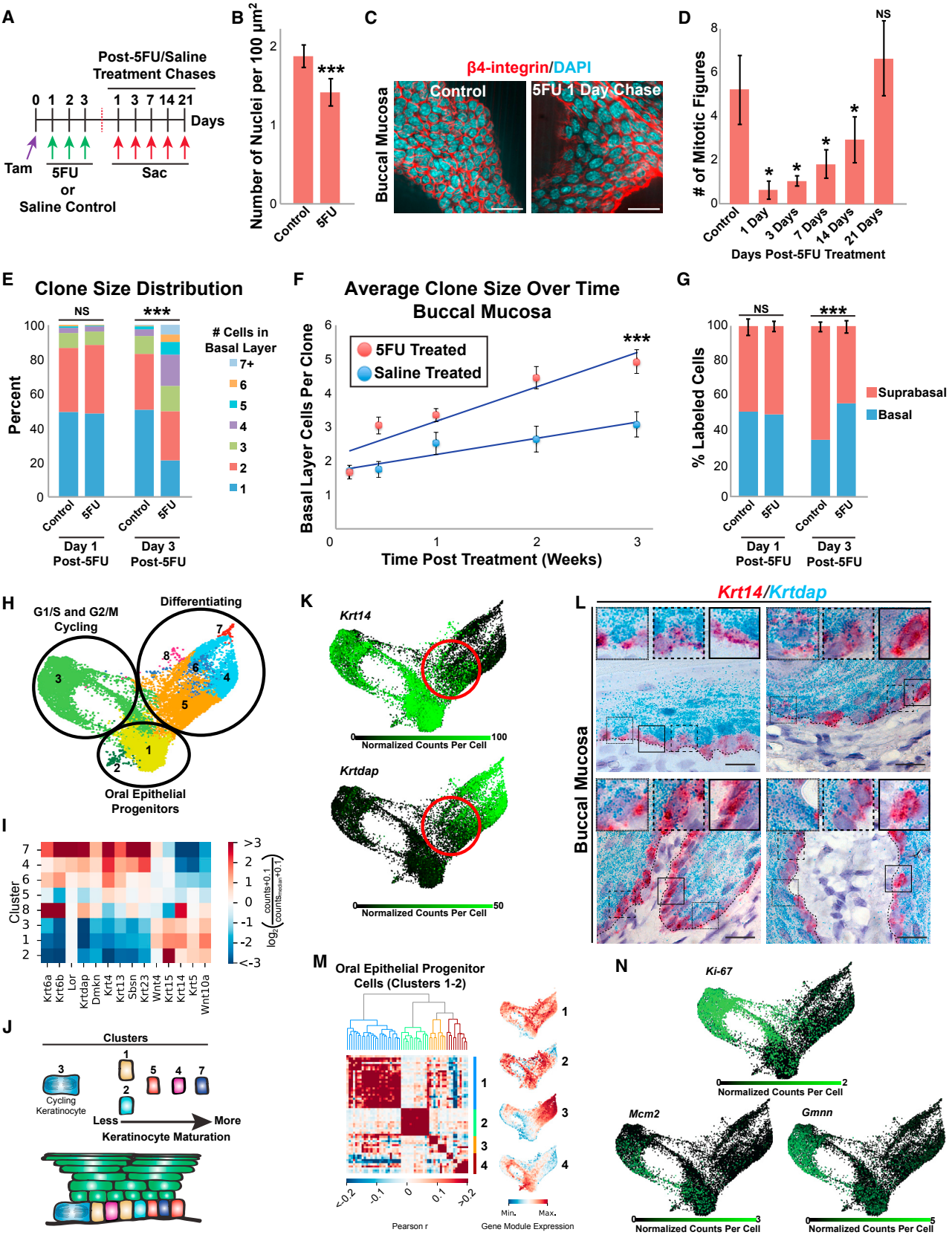

(legend on next page)

inflammation, and keratinocyte migration (Tables S2 and S3). When pooled together, differentiating cells in clusters 4–8 were enriched for transcription factors important for keratinocyte maturation. Thus, cells from these clusters appear to represent a continuum of maturing keratinocytes within the basal layer, which is supported by their sequential organization on the SPRING plot. Based on our earlier kinetics analysis, we predicted that up to 50% of the cells would appear post-mitotic, and indeed, the five putatively post-mitotic clusters comprised about 40% of the cells.

ISH Confirms the Presence of Multiple Basal Layer Cell States Predicted by scRNA-Seq

The structure of the scRNA-seq data suggested that, collectively, the clusters represented a continuum of cell states at various stages of maturation, ranging from OEPCs to post-mitotic cells preparing to leave the basal layer. This was supported by the co-expression patterns of genes identified in the enrichment analysis that were associated with OEPCs and differentiating keratinocytes. For example, *Krt14* (associated with OEPCs) and *Krtdap* (associated with differentiating keratinocytes) showed overlapping mRNA expression patterns despite being enriched within different clusters (Figures 4I and 4K; see Mendeley Figure S2 for other examples). Further supporting this, we found that cells in each cluster showed overlapping expression of many other genes associated with OEPCs (e.g., *Krt5/14*, *Itga6*, *Itgb4*, and hemidesmosome genes) and early differentiating keratinocytes (e.g., *Krt4/13*, *Krtdap*, and multiple genes from the epidermal differentiation complex; see Mendeley Table S1). Importantly, none of the clusters showed expression of late cornified envelope genes such as *Lce1* and *Lce3*, indicating that the post-mitotic basal layer cells fated for differentiation had not yet begun to express the transcripts found in terminally mature keratinocytes. Last, modules of co-expressed genes enriched within OEPCs, cycling cells, and differentiating cells were expressed in several clusters and overlapped with one another (Figures 4M, S2E, and S2F; Table S4).

To confirm these findings, we performed dual-labeled RNAscope ISH to analyze the expression of *Krt14* and *Krtdap* within individual basal layer cells. Similar to the SPRING plot, we identified three main patterns: cells with high levels of *Krtdap* and little expression of *Krt14*, cells with moderate levels of both *Krtdap* and *Krt14*, and cells with low levels of *Krtdap* and high levels of *Krt14* (Figure 4L). ISH for *Wnt4*, *Wnt10a*, and *Krt15* similarly showed cells with high, intermediate, and low expression (Figure S1J). Additionally, we found that *Krtdap*+/*Krt14*− cells comprised an average of 10.7% ± 1.0% of basal layer cells (n = 391 cells scored, mean ± sampling error; see Mendeley Figure S3), which is consistent with the percentage of cells (14%) represented by clusters 4 and 7 that have such a gene expression pattern. These results are in line with our scRNA-seq and gene enrichment analyses, and they show that the cell clusters represent a continuum of cell states within the basal layer as cells transition from OEPCs to post-mitotic cells (Figure 4J).

Cell-Cycle Analysis of Basal Layer Cells Reveals Their Highly Proliferative State

We next explored the cycling dynamics of cells within each of the clusters. To do this, we first looked at *Ki-67* gene expression overlaid on the SPRING plot (Figure 4N), which showed the highest level of expression in cluster 3 and lower levels in several other clusters (e.g., 1, 2, 5, and 4). We hypothesized that low levels of *Ki-67* present in OEPCs in clusters 1 and 2 could indicate that these cells were preparing to enter or had recently entered G1/S. Supporting this, *Mcm2,* one of several proteins that bind DNA origins of replication and form pre-replicative complexes, was expressed in many of the OEPCs at high levels, indicating that these cells were actively cycling (Figure 4N; Shreeram and Blow, 2003). Interestingly, cells from clusters 1–3 together represent 61% of all cells in the scRNA-seq analysis, which is comparable with the estimated proportion of progenitor cells reported in the esophageal epithelial basal layer of 65% (Doupé et al., 2012). In contrast, post-mitotic cells in clusters 4 and 5 with low levels of *Ki-67* also expressed low levels of *Gmnn*, a negative regulator of DNA synthesis whose levels rapidly decline following cell cycle exit (Xouri et al., 2004). This could indicate that these cells recently exited the cell cycle (Figure 4N). These results show that the *Ki-67*

Figure 4. 5FU Has Long-Lasting Effects on Buccal Mucosal OEPCs, and scRNA-Seq Reveals the Population Structure of the Basal Layer

(A) 5FU treatment scheme.

(B and C) 5FU caused a significant decrease in basal layer nuclear density within the buccal mucosa of 5FU-treated mice 1 day post-treatment (***p = 0.0002) (B), illustrated in whole-mount sections (C). Bar graphs represent the average number of nuclei per 100 μm^2 ± SD in mice treated with saline or 5FU following a 1-day chase. Scale bars, 20 μm.

(D) Average number of mitotic figures following treatment with 5FU. Bar graphs represent the average number of mitotic figures per area imaged ± SD (1 day, *p = 0.03; 3 days, *p = 0.01; 7 days, *p = 0.01; 14 days, *p = 0.04; 21 days, not significant).

(E) 3 days after the last dose of 5FU, treated mice showed a significant expansion in clone size distribution (***p < 0.001).

(F) Overall average clone sizes ± SD in mice treated with 5FU are larger. The competition rate of basal layer progenitor cells in 5FU-treated mice is approximately double (increase of 1.01 cells/week ± 0.12 SE versus 0.47 cells/week ± 0.08 SE, respectively). Multivariable linear regression analysis showed that both the treatment type (control versus 5FU, ***p < 0.001) and time post-treatment (***p < 0.001) correlated strongly with clone size and, together, accounted for 80% (R^2 = 0.80) of the variance observed in the clone size distribution. Solid lines represent the neutral drift predictions for clonal growth.

(G) 5FU-treated mice show a significant decrease in the percentage of labeled suprabasal layer keratinocytes. Bar graphs represent the percentage of labeled basal and suprabasal layer keratinocytes 1 and 3 days post-5FU treatment (error bars represent the 95% confidence interval; ***p < 0.001).

(H) scRNA-seq analysis of sorted oral epithelial basal layer cells, shown using a SPRING plot visualization, with clusters indicated.

(I) mRNA expression levels for selected genes associated with keratinocyte differentiation within each of the clusters.

(J) Proposed model depicting keratinocyte cell states present within the basal cell layer of the buccal mucosa.

(K) scRNA-seq SPRING plots overlaid with *Krt14* and *Krtdap* gene expression (the greatest area of overlap is circled in red).

(L) Basal layer keratinocytes at various stages of maturation show a continuum of dual *Krtdap* and *Krt14* co-expression, exemplified by cells that are *Krtdap*^{high}/*Krt14*^{low}, *Krtdap*^{moderate}/*Krt14*^{moderate}, and *Krtdap*^{low}/*Krt14*^{high} (insets). Dashed lines represent the basement membrane. Scale bars, 20 μm.

(M) Positively correlated gene modules identified in OEPCs (clusters 1 and 2).

(N) scRNA-seq SPRING plots overlaid with *Ki-67*, *Mcm2*, and *Gmnn* gene expression.

gene is expressed widely among basal layer cells. Given the rapid turnover rate of the oral epithelium and the fact that the Ki-67 protein can persist in cells that have recently exited the cell cycle (Pacal and Bremner, 2012; Sobecki et al., 2017), it is not surprising that up to 95% of basal layer cells showed positive *Ki-67* immunofluorescence at some level (Figures 2B and S1K–S1M).

DISCUSSION

Our data show that *Bmi1* is expressed in most oral epithelial basal layer cells and labels long-lived OEPCs, which are distributed throughout the oral mucosal basal layer. Throughout the buccal and dorsal tongue epithelia, OEPCs rapidly divide and follow the population asymmetry model with neutral drift dynamics. Although these results differ substantially from the current oral mucosa stem cell paradigm, they are in line with work in the interfollicular epidermis and esophageal epithelium, showing that epithelia from distinct developmental lineages use similar progenitor cell organization strategies to maintain tissue homeostasis (Clayton et al., 2007; Doupé et al., 2010, 2012). The differences between our findings and an earlier report in the tongue (Tanaka et al., 2013) are likely in part due to differences in labeling efficiency of the reporter lines as well as due to the high sensitivity and specificity of the RNAscope ISH technique.

We also demonstrate that the effects of 5FU on OEPCs are unexpectedly long-lasting. Mice in our study were given 3 large boluses of 5FU, so it is possible that levels remained elevated within the plasma for an extended period of time, which could explain why mitotic levels within the buccal mucosa slowly increased back to normal instead of transitioning rapidly to a hyperproliferative state. Additionally, 5FU could lead to continued cell cycle arrest even after levels significantly drop in the plasma. These extended effects on OEPCs, in addition to the complex milieu of signaling factors at the sites of mucosal damage, could help explain why oral mucositis, a common side effect of chemotherapy, can take as long as 2–4 weeks to resolve following the last dose of chemotherapy (Lalla et al., 2008).

Last, the scRNA-seq results show that the oral epithelial basal layer is comprised of both OEPCs and post-mitotic cells that have begun the process of differentiating prior to leaving the basal layer, as seen by the expression of differentiation genes in clusters 4–8. We cannot entirely exclude the possibility that a few suprabasal layer cells were included in these clusters despite sorting only cells with the highest levels of β4-integrin (Figure S4E). One should therefore consider that some of the latest transcriptional events seen in our data, associated with just a few percent of the cells, could have been due to the presence of suprabasal layer cells in the analysis. Any differentiated suprabasal layer keratinocytes present would most likely have been assigned to cluster 7 or, less likely, cluster 4, which expressed the highest levels of *Krtdap* and lowest levels of *Krt14*, and together represented only 14% of the total cells sampled. Although a comparable percentage of *Krtdap*+/*Krt14*− cells (10.7%) are present in the basal layer via ISH (Mendeley Figure S3), it is nonetheless possible that some of the cells in these clusters were suprabasal. Even if we excluded clusters 4 and 7 from the analysis, cluster 5 cells still express moderate to high levels of genes associated with both OEPCs and differentiating keratinocytes (Figure 4K; Mendeley Table S1) and clearly represent an abundant, intermediate, transitional cell state. Therefore, the presence of a few suprabasal layer cells in the analysis would not alter our conclusion that post-mitotic cells begin expressing differentiation-associated genes prior to leaving the basal layer.

The conclusion that differentiation begins in the basal layer is consistent with both the clonal analysis, which predicts that up to half of basal cells are post-mitotic, and the mitotic figure orientation analysis, which shows that most OEPCs divide parallel to the basement membrane, resulting in two daughter cells that initially remain within the basal layer. These post-mitotic basal layer cells presumably undergo a decision to exit the basal layer, during which time they may start to downregulate expression of basal layer genes and start to express differentiation-associated genes. Through currently unknown signals following cell division, each daughter cell within the basal layer either retains its identity as an OEPC or begins to terminally differentiate and eventually delaminate. It is not clear at what point during cell division that commitment to differentiation occurs or whether post-mitotic cells still retain the ability to return to an OEPC state, possibly in response to damage within the basal layer. Interestingly, the expression of gene module 1 in cluster 3 cycling cells (Figures S2E and S2F; Table S4), which includes differentiation-associated genes, hints at the possibilities that either commitment to a differentiated state may begin during cell division or that post-mitotic cells can re-enter the cell cycle. The spatial and transcriptional transitions cells undergo as they differentiate and exit the basal layer on their path to becoming mature keratinocytes will be important to explore in the future. Identifying the signals that drive OEPC daughter cell fate behavior will be crucial to understanding how tissue homeostasis is maintained and how OEPCs contribute to oral disease.

STAR★METHODS

Detailed methods are provided in the online version of this paper and include the following:

- KEY RESOURCES TABLE
- CONTACT FOR REAGENT AND RESOURCE SHARING
- EXPERIMENTAL MODEL AND SUBJECT DETAILS
  - Mouse Lines
- METHOD DETAILS
  - *In situ* hybridization
  - Lineage Tracing
  - BMI1 Immunofluorescence
  - BrdU Pulse-Chase Experiment
  - Whole-Mount Immunofluorescence
  - Dual BrdU and EdU Pulse/Chase Labeling
  - $K5^{tTa}$;**tetO-**$H2B^{GFP}$ Label Retention Experiments
  - Measuring Individual Cell Fluorescence Values in $K5^{tTa}$;tetO-$H2B^{GFP}$ Samples
  - Buccal Mucosa Single Cell Dissociation and FACS Sorting
  - Single Cell RNaseq
  - Imaging Equipment and Software
- QUANTIFICATION AND STATISTICAL ANALYSIS
  - Ki-67 Quantification
  - Cell Cycle Calculations Using BrdU and EdU Dual Labeling

SUPPLEMENTAL INFORMATION

Supplemental Information includes four figures and four tables and can be found with this article online at https://doi.org/10.1016/j.stem.2018.10.015.

ACKNOWLEDGMENTS

We thank the members of the Klein laboratory and Drs. Jeff Bush and Kristin Harter for helpful suggestions. We also thank Kaitlin Corbin from the UCSF Biological Imaging Development Center for help with imaging. This research was funded by NIH R35-DE026602 and U01-DK103147 and Tobacco-Related Disease Research Program (University of California) 587629 (to O.D.K.). K.B.J. was funded by NIH F30-DE022509 and KL2-TR001870. A.M.K. was funded by a Burroughs Wellcome Fund CASI award and an Edward J. Mallinckrodt fellowship.

AUTHOR CONTRIBUTIONS

K.B.J., A.M.K., and O.D.K. designed and performed the experiments, analyzed the data, and wrote the manuscript. S.F. performed sorting and RNA-seq experiments. P.M. and R.Z. analyzed the scRNA-seq data. H.M. and R.D. performed lineage tracing experiments. H.P. wrote the software used for clonal analysis.

DECLARATION OF INTERESTS

A.M.K. is a founder of 1CellBio, Inc.

Received: September 29, 2017
Revised: May 19, 2018
Accepted: October 10, 2018
Published: November 21, 2018

REFERENCES

Arai, Y., Pulvers, J.N., Haffner, C., Schilling, B., Nüsslein, I., Calegari, F., and Huttner, W.B. (2011). Neural stem and progenitor cells shorten S-phase on commitment to neuron production. Nat. Commun. *2*, 154.

Baydar, M., Dikilitas, M., Sevinc, A., and Aydogdu, I. (2005). Prevention of oral mucositis due to 5-fluorouracil treatment with oral cryotherapy. J. Natl. Med. Assoc. *97*, 1161–1164.

Clayton, E., Doupé, D.P., Klein, A.M., Winton, D.J., Simons, B.D., and Jones, P.H. (2007). A single type of progenitor cell maintains normal epidermis. Nature *446*, 185–189.

DeWard, A.D., Cramer, J., and Lagasse, E. (2014). Cellular heterogeneity in the mouse esophagus implicates the presence of a nonquiescent epithelial stem cell population. Cell Rep. *9*, 701–711.

Doupé, D.P., Klein, A.M., Simons, B.D., and Jones, P.H. (2010). The ordered architecture of murine ear epidermis is maintained by progenitor cells with random fate. Dev. Cell *18*, 317–323.

Doupé, D.P., Alcolea, M.P., Roshan, A., Zhang, G., Klein, A.M., Simons, B.D., and Jones, P.H. (2012). A single progenitor population switches behavior to maintain and repair esophageal epithelium. Science *337*, 1091–1093.

Engeland, C.G., Bosch, J.A., Cacioppo, J.T., and Marucha, P.T. (2006). Mucosal wound healing: the roles of age and sex. Arch. Surg. *141*, 1193–1198.

Keyes, B.E., Segal, J.P., Heller, E., Lien, W.-H., Chang, C.-Y., Guo, X., Oristian, D.S., Zheng, D., and Fuchs, E. (2013). Nfatc1 orchestrates aging in hair follicle stem cells. Proc. Natl. Acad. Sci. USA *110*, E4950–E4959.

Klein, A.M., Doupé, D.P., Jones, P.H., and Simons, B.D. (2007). Kinetics of cell division in epidermal maintenance. Phys. Rev. E Stat. Nonlin. Soft Matter Phys. *76*, 021910.

Klein, A.M., Mazutis, L., Akartuna, I., Tallapragada, N., Veres, A., Li, V., Peshkin, L., Weitz, D.A., and Kirschner, M.W. (2015). Droplet barcoding for single-cell transcriptomics applied to embryonic stem cells. Cell *161*, 1187–1201.

Lalla, R.V., Sonis, S.T., and Peterson, D.E. (2008). Management of oral mucositis in patients who have cancer. Dent. Clin. North Am. *52*, 61–77, viii.

Li, L., and Clevers, H. (2010). Coexistence of quiescent and active adult stem cells in mammals. Science *327*, 542–545.

Lim, X., Tan, S.H., Koh, W.L.C., Chau, R.M.W., Yan, K.S., Kuo, C.J., van Amerongen, R., Klein, A.M., and Nusse, R. (2013). Interfollicular epidermal stem cells self-renew via autocrine Wnt signaling. Science *342*, 1226–1230.

Liu, S., and Trapnell, C. (2016). Single-cell transcriptome sequencing: recent advances and remaining challenges. F1000Res. *5*, 5.

Mackenzie, I.C. (1997). Retroviral transduction of murine epidermal stem cells demonstrates clonal units of epidermal structure. J. Invest. Dermatol. *109*, 377–383.

Macosko, E.Z., Basu, A., Satija, R., Nemesh, J., Shekhar, K., Goldman, M., Tirosh, I., Bialas, A.R., Kamitaki, N., Martersteck, E.M., et al. (2015). Highly Parallel Genome-wide Expression Profiling of Individual Cells Using Nanoliter Droplets. Cell *161*, 1202–1214.

Martynoga, B., Morrison, H., Price, D.J., and Mason, J.O. (2005). Foxg1 is required for specification of ventral telencephalon and region-specific regulation of dorsal telencephalic precursor proliferation and apoptosis. Dev. Biol. *283*, 113–127.

Pacal, M., and Bremner, R. (2012). Mapping differentiation kinetics in the mouse retina reveals an extensive period of cell cycle protein expression in post-mitotic newborn neurons. Dev. Dyn. *241*, 1525–1544.

Potten, C.S. (1974). The epidermal proliferative unit: the possible role of the central basal cell. Cell Tissue Kinet. *7*, 77–88.

Schindelin, J., Arganda-Carreras, I., Frise, E., Kaynig, V., Longair, M., Pietzsch, T., Preibisch, S., Rueden, C., Saalfeld, S., Schmid, B., et al. (2012). Fiji: an open-source platform for biological-image analysis. Nat. Methods *9*, 676–682.

Shreeram, S., and Blow, J.J. (2003). The role of the replication licensing system in cell proliferation and cancer. Prog. Cell Cycle Res. *5*, 287–293.

Sobecki, M., Mrouj, K., Colinge, J., Gerbe, F., Jay, P., Krasinska, L., Dulic, V., and Fisher, D. (2017). Cell-Cycle Regulation Accounts for Variability in Ki-67 Expression Levels. Cancer Res. *77*, 2722–2734.

Tanaka, T., Komai, Y., Tokuyama, Y., Yanai, H., Ohe, S., Okazaki, K., and Ueno, H. (2013). Identification of stem cells that maintain and regenerate lingual keratinized epithelial cells. Nat. Cell Biol. *15*, 511–518.

Tumbar, T., Guasch, G., Greco, V., Blanpain, C., Lowry, W.E., Rendl, M., and Fuchs, E. (2004). Defining the epithelial stem cell niche in skin. Science *303*, 359–363.

Weinreb, C., Wolock, S., and Klein, A.M. (2018). SPRING: a kinetic interface for visualizing high dimensional single-cell expression data. Bioinformatics *34*, 1246–1248.

Xouri, G., Lygerou, Z., Nishitani, H., Pachnis, V., Nurse, P., and Taraviras, S. (2004). Cdt1 and geminin are down-regulated upon cell cycle exit and are over-expressed in cancer-derived cell lines. Eur. J. Biochem. *271*, 3368–3378.

Zhang, H.-M., Liu, T., Liu, C.-J., Song, S., Zhang, X., Liu, W., Jia, H., Xue, Y., and Guo, A.-Y. (2015). AnimalTFDB 2.0: a resource for expression, prediction and functional study of animal transcription factors. Nucleic Acids Res. *43*, D76–D81.

Please cite this article in press as: Jones et al., Quantitative Clonal Analysis and Single-Cell Transcriptomics Reveal Division Kinetics, Hierarchy, and Fate of Oral Epithelial Progenitor Cells, Cell Stem Cell (2018), https://doi.org/10.1016/j.stem.2018.10.015

STAR★METHODS

KEY RESOURCES TABLE

REAGENT or RESOURCE	SOURCE	IDENTIFIER
Antibodies		
Rat anti-mouse β4-integrin (1:100 dilution)	Bioscience	553745, 346-11A clone; RRID:AB_395027
Rabbit anti-mouse kI-67 (1:100 dilution)	ThermoScientific	RM-9106-S1, SP6 clone; RRID:AB_149792
Mouse anti-mouse p53 (1:50 dilution)	Invitrogen	MA5-12453, PAb-122 clone; RRID:AB_11004789
Rabbit anti-mouse Keratin14 (1:500 dilution)	Biolegend	905304, Poly19053 clone; RRID:AB_2616896
Rat anti-mouse CD45 (1:100 dilution)	Biolegend	RRID:AB_312966
Mouse anti-BrdU (1:300 dilution)	Thermo Fisher Scientific	RRID:AB_2536432
Rat anti-BrdU (1:500 dilution)	Abcam	RRID:AB_305426
Rabbit anti-mouse Bmi1 (1:500 dilution)	Cell Signaling	RRID:AB_10838137
Goat anti-rat IgG Alexa Fluor-488 (1:400 dilution)	Invitrogen	A-11006; RRID:AB_2534074
Goat anti-rabbit IgG Alexa Fluor-568 (1:400 dilution)	Invitrogen	A-11011; RRID:AB_143157
Goat anti-mouse IgG Alexa Fluor-488 (1:400 dilution)	Invitrogen	A-11001; RRID:AB_2534069
Goat anti-rabbit IgG Alexa Fluor-633 (1:400 dilution)	Invitrogen	A-21070; RRID:AB_2535731
Rabbit anti-rat IgG Alexa Fluor-488 (1:400 dilution)	Thermo Fisher Scientific	RRID:AB_2535796
Biotinylated Rabbit anti-rat IgG (1:500 dilution)	Vector Laboratories	RRID:AB_10015300
Biotinylated Goat anti-rabbit IgG (1:500 dilution)	Vector Laboratories	RRID:AB_2313606
FITC conjugated Rat anti-mouse CD104 (β4-integrin, 1:100)	Biolegend	RRID:AB_2234035
Rat IgG2a kappa FITC Isotype Control (1:100)	Biolegend	RRID:AB_2736919
Critical Commercial Assays		
Click-iT EdU Alexa Fluor 647 kit	ThermoFisher	C10340
Chromium Single Cell 3′ reagent kit v2	10X Genomics	PN-120237
SBS Kit v2	Illumina	FC-402-4021
RNAscope 2.0 detection kit	ACD	310036
RNAscope 2.5 HD Red detection kit	ACD	322350
RNAscope 2.5 HD Duplex detection kit	ACD	322430
Probe-Mm-Bmi1	ACD	312181, lot 16299A
Probe-Mm-K14-C2	ACD	422521-C2, lot 17082C
Probe-Mm-Krtdap	ACD	500671, lot 17083B
Probe-Mm-Wnt4	ACD	401101, lot 17086B
Probe-Mm-Wnt10a	ACD	401061, lot 17215A
RNAscope Negative Control Probe-DapB	ACD	310043, lot 15295A
DIG RNA Labeling Kit (SP6/T7)	Roche	11175025910
TSA Plus Cyanine 3 System	PerkinElmer	NEL744001KT
Deposited Data		
Supplementary Mendeley Figures	https://doi.org/10.17632/52fxfdcb5z.1	N/A
Single cell analysis of oral mucosa basal layer cells scRNaseq dataset	GEO: GSE120654	N/A
Experimental Models: Mouse Lines		
subsection: C57BL/6J	Jackson Laboratory	000664
Bmi1$^{tm1(cre/ESR1)Mrc}$	Jackson Laboratory	010531
Sox2$^{tm1(cre/ERT2)Hoch}$	Jackson Laboratory	017593
Gli1$^{tm3(cre/ERT2)Alj}$	Jackson Laboratory	007913
Lrig1$^{tm1.1(cre/ERT2)Rjc}$	Jackson Laboratory	018418

(*Continued on next page*)

Continued

REAGENT or RESOURCE	SOURCE	IDENTIFIER
Tg(KRT14-cre/ERT)20Efu	Jackson Laboratory	005107
Gt(ROSA)26Sor$^{tm14(CAG-tdTomato)Hze}$	Jackson Laboratory	007914
Tg(tetO-HIST1H2BJ/GFP)47Efu	Jackson Laboratory	005104
Tg(KRT5-tTA)1216Glk/Nci	National Cancer Institute Mouse Repository	MGI 3575755
Software and Algorithms		
FIJI	Schindelin et al., 2012	N/A
Imaris MicroMagellan Compiler plugin for FIJI	https://github.com/henrypinkard/Micro-Magellan	N/A
Adobe Illustrator CS6	Adobe	N/A
SPRING Viewer	https://github.com/AllonKleinLab/SPRING_dev	N/A
Python 2.7	https://www.python.org	N/A

CONTACT FOR REAGENT AND RESOURCE SHARING

Further information and requests for reagents may be directed to and will be fulfilled by lead contact, Ophir Klein (ophir.klein@ucsf.edu)

EXPERIMENTAL MODEL AND SUBJECT DETAILS

Mouse Lines

Mice were housed in accordance with University of California San Francisco Institutional Animal Care and Use Committee (IACUC) guidelines. The UCSF Institutional Animal Care Use Committee approved all mouse experiments. The following mouse lines were obtained from The Jackson Laboratory: C57BL/6J, *Bmi1$^{tm1(cre/ESR1)Mrc}$* (referred to as *Bmi1^{CreER}*), *Sox2$^{tm1(cre/ERT2)Hoch}$* (referred to as *Sox2^{CreER}*), *Gli1$^{tm3(cre/ERT2)Alj}$* (referred to as *Gli1^{CreER}*), *Lrig1$^{tm1.1(cre/ERT2)Rjc}$* (referred to as *Lrig1^{CreER}*), *Tg(KRT14-cre/ERT)20Efu* (referred to as *K14^{CreER}*), *Gt(ROSA)26Sor$^{tm14(CAG-tdTomato)Hze}$* (referred to as *R26^{tdTomato}*), and *Tg(tetO-HIST1H2BJ/GFP)47Efu* (referred to as tetO-*H2B^{GFP}*). *Tg(KRT5-tTA)1216Glk/Nci* mice (referred to as *K5^{tTa}*) were obtained from the National Cancer Institute Mouse Repository. *Bmi1^{CreER}*, *Sox2^{CreER}*, *Gli1^{CreER}*, *Lrig1^{CreER}*, and *K14^{CreER}* mice were crossed with *R26^{tdTomato}* mice (which when transcribed would lead to expression of red fluorescent protein [RFP]) to generate heterozygotes for each allele that were then used for lineage tracing and clonal analysis experiments. *K5^{tTa}* heterozygous mice were crossed with tetO-*H2B^{GFP}* heterozygous mice to generate *K5^{tTa}*; tetO-*H2B^{GFP}* heterozygotes, which were used in label retaining experiments.

METHOD DETAILS

In situ hybridization

RNAscope 2.0 and 2.5 HD Red (ACD, 310036, 322350) and RNAscope 2.5 HD Duplex (ACD, 322430) detection kits were used following the manufacturer's instructions. 2-3 month old C57BL/6J male and female mice (n = 6 mice, repeated 3 times) were euthanized and their oral mucosa/tongue tissues removed and placed into 10% neutral buffered formalin solution at room temperature for ~20 hours. Tissues were then washed 3x5 minutes in phosphate buffered saline (PBS), submitted for paraffin processing, and embedded in paraffin blocks. 5 μm sections were used for all experiments. Sections were boiled in the target retrieval solution at ~100°C for 15 minutes and incubated in the protease plus solution at 40°C for 15 minutes. *Bmi1*, *Krt14*, *Krtdap, Krt15, Wnt4 and Wnt10a* probes specific for *Mus musculus* were purchased from ACD. DapB (purchased from ACD) was used as a negative control along with appropriate positive controls in each experiment. Negative controls consistently showed little to no background staining. RNA *in situ* hybridization was performed in 2-3 month old C57BL/6J male and female mice (n = 3 mice, repeated 3 times) using an anti-*Sox2* digoxigenin-labeled probe on frozen tissue sections using standard protocols. Anti-*Sox2* probes were generated by amplifiying a 750 bp *Sox2* gene fragment cloned within a pBluescript SK+ vector using the DIG RNA Labeling Kit (Roche, 11175025910) according to the manufacturer's instructions. Prior to probe generation, the vector was linearized with a XhoI restriction enzyme and transcribed using a T3 RNA polymerase.

Lineage Tracing

Adult male and female mice ($n \geq 2$ for each time point) greater than 2 months old were given a single intraperitoneal injection of tamoxifen or corn oil (for negative controls) and then euthanized at various times post-treatment (see main text for exact chase time points). Mice were dosed as follows:

Genotype	Tamoxifen Dose Range
Bmi1^{CreER};*R26*^{tdTomato}	1-5mg/25 g
Gli1^{CreER};*R26*^{tdTomato}	3mg/25 g
Lrig1^{CreER};*R26*^{tdTomato}	3mg/25 g
Sox2^{CreER};*R26*^{tdTomato}	0.3-1mg/25 g
K14^{CreER};*R26*^{tdTomato}	0.04mg/25 g

Following euthanization, each mouse was perfused with cold 4% paraformaldehyde (PFA) dissolved in PBS. Oral mucosa, tongue, and skin were then removed and incubated in 4% PFA at 4°C on a shaker for about 2-3 hours. The tissues were then washed 3x5 minutes in PBS and incubated overnight in a 30% (w/v) sucrose-PBS solution at 4°C. The following day, the tissues were embedded and frozen in optimal cutting temperature (OCT) medium (FisherScientific, 50-363-579). 7 μm cryosections were cut and air-dried onto glass slides, washed 3x5 minutes in PBS with 0.1% (v/v) Tween 20 (PBS-T) to remove residual OCT medium, blocked in an animal-free blocking solution (Vector Laboratories, SP-5030) for 1 hour at room temperature, incubated overnight at 4°C with β4-integrin primary antibody, washed 3x10 minutes with PBS-T, incubated with a secondary antibody at room temperature for one hour, washed 2x5 minutes with PBS, stained with 4,6-diamidino-2-phenylindole (DAPI; 5μg/mL, Sigma, D9564-10MG) dissolved in PBS for 30 minutes at room temperature, washed with PBS, mounted with Vectashield Antifade Mounting Medium (Vector Laboratories, H-1000), and sealed with clear nail polish.

BMI1 Immunofluorescence

5 μM sections were cut from formalin-fixed, paraffin-embedded oral mucosal tissues collected from C57BL/6J male and female mice. Sections were rehydrated and antigen retrieval performed by incubating tissues in antigen retrieval buffer (pH 6.0) containing 10 mM citric acid, 2mM ethylenediaminetetraacetic acid (EDTA), and 0.05% (v/v) Tween 20 just below 100°C for 20 minutes followed by a 30 minute cool-down to room temperature. Sections were then incubated with animal-free blocking solution for 30 minutes at room temperature followed by overnight incubation with anti-BMI1 primary antibody at 4°C. Samples were washed 3x5 minutes in wash buffer (PBS with 0.1% (v/v) Triton-X) followed by incubation with biotin-conjugated secondary antibody (Vector Laboratories, BA-1000) for one hour at room temperature. Sections were then incubated with ABC Elite reagent (Vector Laboratories, PK-6100) for 30 minutes at room temperature, washed 3x5 minutes in wash buffer, incubated with the TSA Plus Cyanine 3 System kit (Perkin Elmer Life Sciences, NEL744001Kt) for 10 minutes, and washed 3x5 minutes in wash buffer. Sections were then stained with DAPI dissolved in PBS for 30 minutes at room temperature, washed 3x5 minutes with PBS, mounted with Vectashield Antifade Mounting Medium, and sealed with clear nail polish.

BrdU Pulse-Chase Experiment

3 month old wild-type C57BL/6J male and female mice ($n \geq 2$ for each time point) were given an intraperitoneal injection of 1mg of 5-bromo-2′-deoxyuridine (BrdU) dissolved in PBS and then euthanized at various time points post-treatment (see main text for exact chase time points). After being euthanized, each mouse was perfused with cold 4% PFA dissolved in PBS. The oral mucosa and tongue were then removed and incubated in 4% PFA overnight at 4°C. The next day, the tissues were washed 3x5 minutes in PBS, submitted for paraffin processing, and then embedded in paraffin blocks. 5 μm sections were used for the subsequent BrdU immunohistochemistry experiments following standard protocols. Briefly, slides were deparaffinized, an antigen retrieval step was performed using a citrate buffer (Vector Unmasking Solution, Vector Laboratories, H-3300) in a pressure cooker for 15 minutes, washed 4x5 minutes in distilled water, washed in PBS for 5 minutes, incubated in 3% (v/v) hydrogen peroxide diluted in PBS for 30 minutes at room temperature, washed in PBS for 5 minutes, incubated in 0.2N hydrochloric acid for 45 minutes at 37°C, washed again in PBS for 5 minutes, washed for 5 minutes in PBS-T, blocked in blocking buffer (5% bovine serum albumin, 5% bovine serum, 0.1% Triton-X dissolved in PBS) for 1 hour at room temperature, incubated with an anti-BrdU primary antibody overnight at 4°C, washed 3x10 minutes in PBS-T, incubated with a biotinylated rabbit anti-rat secondary antibody at room temperature, and washed 3x10 minutes in PBS. The Vectastain Elite ABC HRP Kit (Vector Laboratories, PK-6100) was used to develop the slides following the manufacturer's protocol. Appropriate positive and negative controls were run during each experiment.

Whole-Mount Immunofluorescence

Mice were euthanized and the buccal mucosa and tongue quickly removed, rinsed in PBS without magnesium or calcium, and placed in a pre-warmed (37°C) solution of 20mM EDTA dissolved in PBS without magnesium or calcium. The buccal mucosa was incubated for 2 hours and the tongue for 4 hours at 37°C. Following incubation, the epithelium was peeled and separated from the underlying connective tissue, rinsed in PBS, fixed for one hour at room temperature or overnight at 4°C in 4% PFA, washed 3x5 minutes in PBS, and stored in PBS with 0.02% sodium azide at 4°C. For immunofluorescence staining, the separated epithelial sheets were incubated in whole-mount blocking/permeabilization buffer (1% bovine serum albumin, 5% horse serum, 0.8% Triton-X) for 1-3 hours at room temperature, incubated with a primary antibody diluted in the blocking buffer overnight at 4°C, washed 3x15 minutes in PBS-T, incubated with a secondary antibody for one hour at room temperature or overnight at 4°C, washed 2x15 minutes in PBS-T, stained with

DAPI dissolved in PBS for 30 minutes at room temperature, washed 2x5 minutes in PBS, and mounted basal layer side up (i.e., touching the coverslip) onto a glass slide using Vectashield Antifade Mounting Medium, and sealed with clear nail polish. Multiple sections of tissue from each mouse described in the main text/methods were used in each staining experiment.

Dual BrdU and EdU Pulse/Chase Labeling

To assess cell cycle duration, 8 week old C57BL/6J female mice (n = 4 mice) were used to calculate the average lengths of both the S-phase (3121 cells) and overall cell cycle times (40726 cells) using a dual BrdU/EdU labeling technique described comprehensively previously (Martynoga et al., 2005). Briefly, mice were first given an intraperitoneal injection with 0.75 mg/25 g of 5-ethynyl-2′-deoxyuridine (EdU), followed 1.5 hours later by an intraperitoneal injection with 0.75mg/25 of BrdU. Mice were then euthanized 30 minutes later, 2 hours from the first injection with EdU (see Figure 2E). Epithelial sheets were prepared from the buccal mucosa of each mouse as already described. Buccal mucosal epithelium was then blocked for 3 hours in whole-mount blocking/permeabilization buffer, incubated in 1N hydrochloric acid diluted in water for 20 minutes at 37°C, washed 4x5 minutes in PBS-T, and stained for EdU using the Click-iT EdU Alexa Fluor 647 kit following the manufacturer's instructions (ThermoFisher, C10340). Following staining, the samples were washed 3x10 minutes in PBS-T, incubated overnight at 4°C in a specific anti-BrdU antibody that does not cross-react with EdU, washed 3x15 minutes in PBS-T, incubated with a secondary antibody for one hour at room temperature, washed 3x15 minutes in PBS-T, stained with DAPI for 30 minutes at room temperature, washed 1x5 minutes in PBS, mounted onto glass slides as already described, and sealed with clear nail polish. To assess reentry of cells into the cell cycle, 3 month old male and female C57BL/6J mice (n = 3 mice) were given a single injection of BrdU, a second injection of EdU after 48 hours, and then euthanized 3 hours later (51 hours following the BrdU injection). The buccal mucosa was isolated, epithelium separated from the underlying connective tissue, and probed for BrdU and EdU expression as already described.

$K5^{tTa}$;tetO-$H2B^{GFP}$ Label Retention Experiments

2 to 4 month old male and female $K5^{tTa}$;tetO-$H2B^{GFP}$ mice were used ($n \geq 3$ mice per chase time point). To inhibit expression of the tetO-$H2B^{GFP}$ allele, mice were initially given an intraperitoneal injection of doxycycline (0.4mg, Enzo Life Sciences, ALX-380-273-G005) and were then maintained on mouse chow that contained doxycycline (200mg/kg, BioServ, S3888). Mice were subsequently euthanized at 0 days (baseline), 3 days, 7 days, 21 days, 6 weeks, and 3 months after doxycycline treatment. The buccal mucosa in each mouse was removed, the epithelium separated from the underlying connective tissue, stained with DAPI in PBS for 30 minutes at room temperature, rinsed 2x5 minutes in PBS, and mounted onto glass slides as already described. Tissues were imaged in two ways. First, confocal microscope settings (e.g., laser power, exposure time, binning, gain, etc.) were adjusted to maximize the EGFP signal in the baseline $K5^{tTa}$;tetO-$H2B^{GFP}$ samples (i.e., did not receive any doxycycline), without over-exposing them and over-saturating the microscope camera. These same microscopic imaging parameters were then used to image the remaining $K5^{tTa}$;tetO-$H2B^{GFP}$ samples in order to determine the relative differences in fluorescence between them. Next, optimized confocal settings were adjusted for each sample to maximize EGFP expression in order to detect any rare, label retaining cells at later chase time points.

Measuring Individual Cell Fluorescence Values in $K5^{tTa}$;tetO-$H2B^{GFP}$ Samples

Using the confocal images taken with identical imaging parameters for each $K5^{tTa}$;tetO-$H2B^{GFP}$ sample, the total relative fluorescence values for individual basal layer keratinocytes were calculated in FIJI (baseline: n = 2 mice, 2173 cells; 3 day chase: n = 6 mice, 4797 cells; 7 day chase: n = 3 mice, 3030 cells). Relative fluorescence values were calculated by manually tracing individual cell nuclei (the location of the GFP signal) and then measuring the IntDen output under the analyze menu in FIJI. The IntDen function multiplies the mean fluorescence (i.e., mean pixel intensity) within a specified region of interest by its area (i.e., number of pixels). In this way, the total relative fluorescence takes into account both nuclear size and mean pixel intensity. Background subtraction was also applied to each sample to control for low levels of background fluorescence.

Buccal Mucosa Single Cell Dissociation and FACS Sorting

Freshly dissected buccal mucosae from 12 week old female C57BL/6J mice (n = 10 mice) were incubated in EDTA (20mM) and PBS without calcium or magnesium for 90 min at 37°C, and the epithelium peeled away from the connective tissues. The epithelial sheets were minced into small pieces and incubated in DMEM/F12 (GIBCO, 11039-021) with 1% penicillin/streptomycin (GIBCO, 15140-122), 30ug/ml DNase I (Worthington, LS002007), 3 mg/ml collagenase P (Sigma, 11213857001) for 30 min at 37°C with intermittent shaking to help dissociate the cells. Cells were then filtered through a 40 μm filter (Falcon, 352340) into FACS buffer (DMEM/F12 medium with 5% fetal bovine serum, 10mM HEPES, and 2.5mM EDTA), spun down at 4°C, and resuspended in FACS buffer with Fluorescein isothiocyanate (FITC) labeled anti-mouse CD104 (β4-integrin) antibodies (as previously described in DeWard et al., 2014) and incubated for 30 minutes on ice in the dark. Cells were then spun down at 4°C, resuspended in FACS buffer, and sorted on a FACSAria II cell sorter (Becton Dickinson). Prior to sorting, dead cells and debris were stained with DAPI (0.5ug/mL) and excluded. An appropriate antibody isotype control was also used.

Single Cell RNaseq

Sorted, individual cells positive for high levels of β4-integrin expression were run in two lanes (i.e., two technical replicates) at different loading concentrations on the Chromium Controller (10X Genomics) using the Chromium Single Cell 3′ Reagent Kit v2 (10X

Genomics, PN-120237) according to the manufacturer's instructions. The resulting cDNA library was then sequenced on an Illumina HiSeq 2500 (Illumina) using the HiSeq 2500 Rapid Run with SBS Kit v2 (Illumina, FC-402-4021).

Imaging Equipment and Software

Whole-mount tissues and cryosections were imaged at room temperature on one of two microscopes: an inverted Zeiss confocal microscope with a Yokogawa CSU-10 spinning disc and Andor iXon EMCCD camera using a Zeiss Plan-NeoFluar 40x (NA: 1.3) 1022-818 oil immersion objective or with an inverted Zeiss Spinning Disc with a Yokogawa CSU-X1 spinning disc and Axiocam 506 CCD camera using a Zeiss 40x (NA: 1.1) LD C-Apochromat water immersion objective. FFPE sections were imaged on an upright Leica DM5000B microscope with a Leica DFC 500 camera and using 40x (NA: 0.75) HCX PL S-APO air objective or a 63x (NA: 1.3) HCX PL APO oil objective. All image analysis was performed using FIJI (Schindelin et al., 2012). Figures were created using Adobe Illustrator CS6.

QUANTIFICATION AND STATISTICAL ANALYSIS

Ki-67 Quantification

10 week old male and female C57BL/6J mice (n = 5 mice, 6123 cells; referred to as "young mice" in main text) were used to quantify the percentage of Ki-67 positive basal layer keratinocytes in the buccal mucosal epithelium for the experiments described in Figure 2. 18-19 month old male *Bmi1*^{CreER};*R26*^{tdTomato} mice (n = 3 mice, 5154 cells; referred to as "old mice" in the main text) were used to quantify the percentage of Ki-67 positive basal layer keratinocytes in the buccal mucosal epithelium for the experiments described in Figure 3. In both instances, separated epithelial sheets were stained for CD45 and Ki-67 and mounted as already described. In order to accurately count the number of keratinocytes present, CD45 (expressed on all mature hematopoietic cells except for mature erythrocytes), was used to highlight resident immune cells so that they would be excluded from the analysis. The number of Ki-67 positive cells as a percentage of the total number of cells was quantified manually using FIJI. A nonparametric Wilcoxon rank-sum two-tailed test with a significance level of 0.05 was used to compare the percentages of Ki-67 positive basal layer keratinocytes found in the "young mouse" (10 week old) samples with the percentages obtained from the "old mouse" (18-19 month old) samples. Multiple imaged areas from each sample were evaluated for this analysis.

Cell Cycle Calculations Using BrdU and EdU Dual Labeling

Following injection with EdU and BrdU, cells that have exited the S-phase prior to euthanasia will only label with EdU whereas cells still within the S-phase when the mouse is euthanized will be labeled with both EdU and BrdU (see Figure 2F). For the calculations, it was assumed that EdU and BrdU did not reach detectable levels within tissues for 30 minutes following injection into the mouse. Using the formulas below as previously described by Martynoga et al. (2005), the average length of S-phase was calculated first, which was then used to calculate the average overall cell cycle length. The average percent of Ki-67 positive keratinocytes calculated in Figure 3J (95.05%) was used to estimate the number of cycling cells in each area (P_{cells}) imaged/analyzed when calculating the average cell cycle time.

$$\frac{\text{Time during which cells can incorporate EdU but not BrdU } (T_i)}{\text{Length of S-Phase } (T_S)} = \frac{\text{Number of cells that leave S-phase during experiment } (\text{EdU}+/\text{BrdU-}) \ (L_{cells})}{\text{Number of cells still in S-phase at the end of the experiment } (\text{EdU}+/\text{BrdU}+) \ (S_{cells})} \quad \therefore \ T_s = T_i\left(\frac{S_{cells}}{L_{cells}}\right)$$

$$\frac{\text{Length of S-phase } (T_s)}{\text{Length of cell cycle } (T_c)} = \frac{\text{Number of cells still in S-phase at the end of the experiment } (\text{EdU}+/\text{BrdU}+) \ (S_{cells})}{\text{Number of proliferating cells in area sampled } (\text{Ki-67}+) \ (P_{cells})}$$

$$\therefore \ T_c = T_s\left(\frac{P_{cells}}{S_{cells}}\right)$$

Clonal Analysis of Buccal Mucosa and Tongue Epithelium

2 to 3 month old ("young") or 15 to 19 month old ("old") male and female *Bmi1*^{CreER};*R26*^{tdTomato} mice (n $\geq$ 3 mice per chase time point) were given a single intraperitoneal injection of tamoxifen (1mg/25 g for clonal analyses in the buccal mucosa and 2mg/25 g for clonal analyses in the tongue) to label single basal layer keratinocytes sufficiently far enough apart so that clonal collisions would be avoided. "Young" mice analyzed for clones within the buccal mucosa were euthanized at 3 days, 5 days, 14 days, 21 days, 28 days, 6 weeks, 3 months, 6 months, and 9.8 months following injection with tamoxifen. "Old" mice analyzed for clones within the buccal mucosa were euthanized at 3 days, 7 days, 14 days, 21 days, 6 weeks, and 3 months following injection with tamoxifen. "Young" mice analyzed for clones within the dorsal tongue epithelium were euthanized at 3 days, 7 days, 21 days, 6 weeks, and 4 months following tamoxifen injection. The buccal mucosa and tongue were then removed and epithelial sheets separated, incubated with an anti-β4-integrin primary antibody and appropriate secondary antibody, and mounted on glass slides as already described. A large grid of overlapping confocal stack tiles (each measuring either 512x512 pixels or 996x996 pixels) was then imaged

for each sample with z stack spacing of 1 μm. Tiles were stitched together using the Imaris MicroMagellan Compiler plugin for FIJI (freely available at http://biomicroscopy.ucsf.edu/mediawiki/index.php?title=Analysis_Software_Repository) and clones analyzed in FIJI. Representative groups of tiles from each sample were then selected and the total number of clones as well as the total number of basal layer keratinocytes per clone quantified. For Figures 3D, 3E, 3G, and 3H, asymptotic fits of a neutral drift model were performed as described previously (Klein et al., 2007; Lim et al., 2013). In brief, the average clone size, $\langle n(t) \rangle$, is predicted to grow linearly, $\langle n(t) \rangle = 1/\rho + (r\lambda/\rho)*t$, where ρ is the fraction of basal cells that divide, λ is the cell cycle rate, and 2r is the fraction of divisions that give rise to daughter cells with a symmetric fate (both dividing or both differentiating). The density of clones in the basal layer, $N_C(t)$, is predicted to drop in a reciprocal manner, $N_C(t) = N_C(0)/(1 + r\lambda*t)$. Numerical fits of the data to these curves were carried out in Microsoft Excel. Statistical significance of the fits is given in the main text. Parameter values are not important to establish the general signature of neutral drift, but are provided for completeness: for the younger adult *Bmi1*^{CreER};*R26*^{tdTomato} mouse labeled clones in the buccal mucosa, we found $r\lambda/\rho$ = 1.7cells/week (Figure 3D), and $r\lambda/N_C(0)$ = 0.22clones/tile/week (Figure 3E). With $N_C(0)$ = 3.9 ± 0.6 clones/tile (mean ± SEM), and λ = 2 days (estimated from H2B-GFP dilution and from EdU/BrdU double-labeling), this gives an estimate of $r \approx 0.23$, $\rho \approx 0.47$. Thus, approximately half of the basal layer is predicted to be post-mitotic, in agreement with results of scRNA-Seq. From these quantities, the exit rate Γ of post-mitotic cells can be shown to be comparable to the cell cycle, because $\Gamma = \rho\lambda/(1\text{-}\rho) \approx \lambda$. For the aged *Bmi1*^{CreER};*R26*^{tdTomato} mice (Figure 3I), the slope values for the average basal layer footprint were $r\lambda/\rho$ = 0.85 cells/week. Finally, for dorsal tongue basal layer keratinocytes in the *Bmi1*^{CreER};*R26*^{tdTomato} mice, the slope values for the average basal layer footprint were $r\lambda/\rho$ = 2.8 cells/week.

Nuclear Density and Clonal Analysis of 5-Fluorouracil Treated Mice

5-Fluorouracil (5FU) powder (Sigma, F6627-5G) was dissolved in sterile 0.85% saline at a concentration of 6.25mg/mL, incubated at 60°C for 45 minutes with intermittent vortexing in order to ensure complete dissolution of the powder into solution, and pH adjusted to 9.2. Aliquots were then frozen at −20°C and thawed only once prior to injection into mice. 8-9 month old male and female *Bmi1*^{CreER};*R26*^{tdTomato} mice (n = 3 mice per chase time point) were first given an intraperitoneal injection with tamoxifen (1mg/25 g) on day 0, and then given 3 sequential intraperitoneal injections of either 0.85% normal saline or 5FU (50mg/kg) on days 1, 2, and 3. Mice were euthanized at days 1, 3, 7, 14, and 21 days following the last dose of saline or 5FU (see Figure 4A). Buccal mucosa was removed, epithelial sheets separated, incubated with anti-β4-integrin/secondary antibodies, and mounted on glass slides as described above. Samples were then imaged and clones analyzed as already described. Additionally, clone size distributions were analyzed in mice at the 1 day chase (control: n = 2 mice, 203 clones; 5FU-treated: n = 3 mice, 507 clones) and at the 3 day chase (control: n = 3 mice, 367 clones; 5FU-treated: n = 3 mice, 292 clones) time points. The number of RFP-labeled suprabasal layer keratinocytes was also quantified at the 1 day chase (control: n = 2 mice, 691 cells; 5FU-treated: n = 3 mice, 1458 cells) and 3 day chase (control: n = 3 mice, 1465 cells; 5FU-treated: n = 3 mice, 1281 cells) time points. Finally, the number of nuclei in the basal layer was quantified at the 1 day chase in control (n = 3 mice, 4021 nuclei) and 5FU-treated mice (n = 3 mice, 3551 nuclei). A nonparametric Wilcoxon rank-sum two-tailed test with a significance level of 0.05 was used to analyze the number of nuclei in control vs. 5FU-treated mice. A chi-squared test with a significance level of 0.05 was used to analyze changes in the clone size distribution of control vs. 5FU-treated mice. A Fisher's exact test with a significance level of 0.05 was used to analyze the frequency of labeled basal and suprabasal layer cells in control vs. 5FU-treated mice.

Mitotic Figure Quantification and Orientation Analysis

Using the whole-mount clonal analysis imaging data collected from the saline or 5FU treated *Bmi1*^{CreER};*R26*^{tdTomato} mice, mitotic figures were identified via histomorphology and their overall number quantified and orientation assessed. Only a portion of the total mitotic figures identified were at a suitable stage of division such that their mitotic orientations could be reliably evaluated. To do this, orthogonal views were created in FIJI for images containing mitotic figures, which permitted the evaluation of each mitotic figure in multiple planes of section in order to establish its proper orientation. Mitotic figures were grouped into one of 5 categories based on the relationship of the dividing cells to the underlying basement membrane (BM), represented by β4-integrin staining, as well as to one another. The categories were as follows: parallel (both mitotic figures touch the BM), oblique (one mitotic figure touches the BM while the other has lifted off at an approximately 45° angle to the remaining mitotic figure), perpendicular (one mitotic figure touches the BM while the other is directly above the underlying mitotic figure), intermediate (one mitotic figure touches the BM while the second is barely touching the BM and appears to be in the process of lifting off), and suprabasal (both mitotic figures have simultaneously lifted off the BM and are no longer touching it). See Figure S4 for examples. Mitotic figures whose orientations could be accurately determined were analyzed in control mice (n = 11 mice, 533 mitotic figures) and 5FU-treated mice (n = 14 mice, 440 mitotic figures). A Fisher's exact test with a significance level of 0.05 was used to compare the frequency of parallel-orientated mitotic figures in the saline treated mice with those in the 5FU treated mice. In order to maximize the sample size for the 5FU treated mice, the mitotic orientation counts from each chase time point were pooled. A nonparametric two-tailed Wilcoxon rank-sum test with a significance level of 0.05 was used to compare the overall number of mitotic figures per field (tile) imaged in the saline treated *Bmi1*^{CreER};*R26*^{tdTomato} mice (n = 11 mice, 1224 mitotic figures [MFs]) with the total number of mitotic figures identified at each of the chase time points in the 5FU treated mice (1 day chase: n = 2 mice, 89 MFs; 3 day chase: n = 3 mice, 159 MFs; 7 day chase: n = 3 mice, 257 MFs; 14 day chase: n = 3 mice, 238 MFs; 21 day chase: n = 3 mice, 383 MFs).

Single Cell RNaseq Data Cleanup and Normalization

Cells with less than 1000 total counts or more than 10% of counts coming from mitochondrial genes were considered low quality and filtered out. The surviving 17,296 transcriptomes had 8,261 total counts on average, and were total-count normalized as described in (Klein et al., 2015). Upon initial visualization and clustering of the data (see below) we identified a small fraction of cells (n = 237) forming well separated clusters and characterized by distinct expression of either immune genes (*Nkg7*, *Csf1r*) or salivary duct markers (*Krt7*). These cells were excluded from further analysis. We applied an additional clean up step to remove doublets (n = 497), which represent rare events of two cells occasionally entering the same droplet during microfluidic barcoding. Briefly, single cell transcriptomes from the dataset are randomly combined to generate *in silico* doublets, which serve as a decoy training set used to train a k-nearest neighbor classifier. Observed cells classified as doublets are removed from further analysis. The detailed method will be published elsewhere. Following clean up and removal of unwanted cell populations, 16,572 cells remained for analysis.

Single Cell RNaseq Data Visualization and Clustering

The high dimensional single cell RNaseq data was visualized in 2D as a force directed layout of a *k* nearest neighbors (*k*NN) graph using SPRING (Weinreb et al., 2018), a method that preserves topological relationships between cells and is therefore well suited to visualize continuous data such as that described here. The plot was divided into clusters using the spectral clustering on the same kNN graph as used for SPRING [implementation in python, sklearn.cluster.SpectralClustering(affinity = 'precomputed', assign_labels = 'discretize')]. First, the graph was divided into 20 clusters. Clusters with high *Ki-67* expression were merged together and labeled as cycling cells. Next, we merged clusters that had less than 2 differentially expressed genes (DEGs). At this step, DEGs were defined as having an absolute fold-change of 5 (after the addition of a pseudo value of 1 count), and statistically significantly different between the two clusters compared (FDR < 0.05, two-tailed Mann-Whitney U test $p < 0.05$). Interactive explorers of the resulting SPRING plots can be accessed here:

Before cleanup (including potential doublets, immune, and salivary duct cells): https://kleintools.hms.harvard.edu/tools/springViewer_1_6_dev.html?datasets/OphirKlein_buccal_mucosa/6_all_cells
After cleanup: https://kleintools.hms.harvard.edu/tools/springViewer_1_6_dev.html?datasets/OphirKlein_buccal_mucosa/6_only_epith_v1

Cell Cluster-Specific Gene Identification

Gene (*g*) was considered specific to cluster (i) if (*g*) was:

a) Detected in at least 3 cells with at least 3 counts (after normalization) across all cells.
b) Statistically significantly higher in cluster (i) compared to all other cells (FDR < 0.05; two-tailed Mann-Whitney U test $p < 0.05$).
c) Expressed 1.5x higher in cluster (i) compared to any other cluster. Before calculating fold-changes, a pseudo value of 0.1 count was added to buffer against low expression and avoid division by zero.

The criteria described above select for genes enriched in a specific population but excludes genes specific for more than one cluster. For example, no exclusive genes were identified for cluster 5, which likely represent less differentiated states in the continuum formed by *Dmkn*^{hi} cells. Therefore, we repeated the selection described above treating clusters 4/5/6/7/8 collectively to identify genes specific to more than one of these clusters. Heatmaps in Figure 4M and Figures S2E and S2F show genes specific to two or more populations from 4/5/6/7/8, followed by genes exclusive to each of the beta4-integrin positive populations identified. Hits are ordered by decreasing max-to-second-max ratio of average expression within clusters. Up to 50 hits are shown per population. A complete enriched gene list with expression levels and p values from statistical testing are provided in Table S2. Transcription factor lists were obtained from animaltfDB (Zhang et al., 2015).

Correlated Gene Module Identification

While dividing the *k*NN graph into clusters provides a convenient summary of distinct transcriptomic states observed in single cell data, it is less suited to capture heterogeneity that manifests as partially overlapping gene expression programs. To address this heterogeneity within continua formed by *Ki-67*^{hi} cells (cluster 3), *Ccnd2*^{hi}*Ki-67*^{low} cells (clusters 1 and 2), and differentiating *Dmkn*^{hi} cells (clusters 4/5/6/7/8), we identified modules of correlated genes as follows:

a) Select only cells of interest, e.g., clusters 4/5/6/7/8 for differentiating basal cells.
b) Identify 2000-3000 of the most variables genes across all selected cells (variability statistic v above mode, as described in (Klein et al., 2015) expressed in at least 5 counts in at least 5 cells, and excluding mitochondrial and ribosomal protein genes.
c) Calculate gene-gene Pearson correlation.
d) Keep gene (*g*) if correlation coefficient r > 0.2 for the nth most correlated gene to (*g*), with n = 5,10,10 for *Ccnd2*^{hi}*Ki-67*^{low}, *Dmkn*^{hi}, and *Ki-67*^{hi} cells, respectively.
e) Hierarchically cluster (correlation distance metric, Ward linkage) surviving genes to reveal discrete blocks of correlated genes (Figure 4M; Figures S2E and S2F).

Each block of correlated genes was collapsed into a single "signature" by taking the mean rank (dense ranking).

Statistical Analysis

All statistical analyses were run using Stata/SE, version 11.2 (StatCorp). Nonparametric two-tailed Wilcoxon rank sum, Chi-Square, and Fisher's exact tests were used with a significance level set at $\alpha = 0.05$. For the clone survival analyses, the clone size distributions were transformed via an inverse function in order to achieve linearity for the subsequent linear regression analyses. Error bars represent either the standard deviation, standard error, or 95% confidence interval, as detailed within the text.

DATA AND SOFTWARE AVAILABILITY

Data Availability

The data that support the findings of this study are available from the corresponding author upon reasonable request.

The accession number for the single cell RNA-seq data reported in this paper is GEO: GSE120654.

Supplemental figures have been deposited to Mendeley online and can be accessed using the following link: https://doi.org/10.17632/52fxfdcb5z.1.

Software Availability

The Imaris MicroMagellan Compiler plugin for FIJI used to analyze the clonal analysis whole-mount images is freely available at http://biomicroscopy.ucsf.edu/mediawiki/index.php?title=Analysis_Software_Repository